

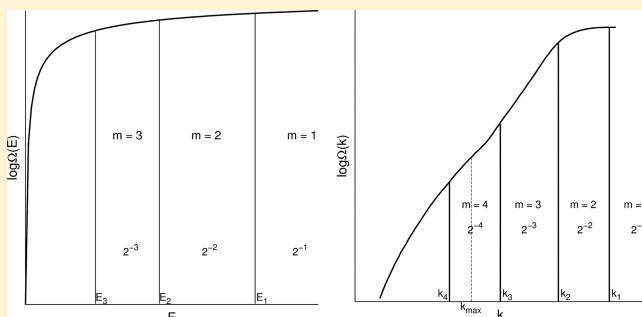
Density of States Partitioning Method for Calculating the Free Energy of Solids

Hainam Do* and Richard J. Wheatley*

School of Chemistry, University of Nottingham, University Park, Nottingham NG7 2RD, U.K.

ABSTRACT: We propose a new simulation method, which combines a cage model and a density of states partitioning technique, to compute the free energy of an arbitrary solid. The excess free energy is separated into two contributions, noninteracting and interacting. The excess free energy of the noninteracting solid is computed by partitioning its geometrical configuration space with respect to the ideal gas. This quantity depends on the lattice type and the number of molecules. The excess free energy of the interacting solid, with respect to the noninteracting solid, is calculated using density of states partitioning and a cage model. The cage model is better than the cell model in that it has a smaller configuration

space and better represents the equilibrium distribution of solid configurations. Since the partition function (and hence free energy) is obtained from the density of states, which is independent of the temperature, equilibrium thermodynamic properties at any condition can be obtained by varying the density. We illustrate our method in the context of the free energy of dry ice.



INTRODUCTION

Computing free energy has been an active field of theoretical research for many decades and still remains a challenge in molecular simulation. Many physical and chemical phenomena can be elucidated from the knowledge of the free energy. Thermodynamic integration¹ is frequently used to determine the free energy difference between two states. However, it can be computationally demanding when applied to systems with large and complex changes, for example, calculation of solvation free energies of large solutes or calculation of the free energy of complex conformational changes. Thus, it is important to develop techniques that can provide the absolute free energy for each state independently, allowing the free energy difference to be calculated even for significantly different states because the integration path is avoided. Efforts toward achieving this goal have been made.^{2,3} However, their applications are relatively limited to simple systems.

Calculating the free energy via the density of states is efficient. As the density of states is independent of the temperature, equilibrium thermodynamic properties at any condition can be obtained from $\Omega(E, \rho)$ by varying the density. Elegant approaches for calculating the density of states have been developed in the past few decades.^{4–8} Most of these were developed for systems with a discrete and finite energy range. When applied to systems with a continuous and infinite energy range, one has to choose a finite range of energy (cutting off the high-energy range) either via trial and error or by calculation.^{9–11} Thus, the partition function can only be computed to within a multiplicative constant. Recently, we have developed a density of states (DOS) partitioning Monte Carlo (MC) technique that can overcome these limitations.^{12,13} The DOS partitioning method calculates the density of configura-

tional energy states, from which the excess partition function and hence the excess free energy of molecular fluids can be obtained. The absolute free energy can be calculated by adding the ideal gas free energy to the excess free energy. The DOS partitioning method has been applied to calculate the free energies of pure and binary mixtures of fluids.^{12,13} A similar technique named "Nested Sampling" has been proposed by Partay et al.¹⁴ and Burkoff et al.¹⁵ to study small Lennard-Jones clusters and simple protein models. The DOS partitioning method is equivalent to Nested Sampling as generalized by Partay et al.¹⁴ with half of the distribution sampled at each step.

The freezing transition properties of model systems and real fluids are of tremendous importance. Since the measurement of these properties is time-consuming and expensive, computer simulation based on molecular modeling is a promising alternative. Thermodynamic integration in combination with a solid model with known free energy has been the most commonly used approach to calculate the freezing transition properties.^{16,17} A weakness of this approach, however, is the possibility of encountering singularities along the integration path, and numerous simulations may be required to traverse the path. In this work, we propose an improved version of the DOS partitioning method together with a new solid model (the cage model) for efficiently computing the absolute free energy of an arbitrary solid. The free energy of the cage model cannot be calculated analytically. However, it can be computed easily by utilizing the DOS partitioning approach.

Of particular interest to us are systems that contain carbon dioxide (CO_2).^{13,18–22} While the fluid phase of CO_2 has been

Received: August 9, 2012

Published: November 16, 2012

extensively studied in molecular simulation, its solid phase has received rather less attention. In this paper, we apply our new DOS partitioning method together with the cage model to calculate the free energy of CO₂ cubic phase I, commonly known as dry ice. We also present the solid–vapor and solid–liquid phase diagram for CO₂. This is a key step to predicting high-pressure structures of CO₂, which have recently attracted much attention.^{23–31}

■ THE DENSITY OF STATES PARTITIONING METHOD

Calculating the Density of States and Partition Functions. The DOS partitioning method^{12,13} divides the configurational energy range recursively into subdivisions (indexed m), working down from infinite energy, such that the integrated normalized density of states $\int_{E_m}^{E_{m-1}} \Omega(E) dE / \int_{-\infty}^{\infty} \Omega(E) dE$ is $1/2^1$ for the first energy subdivision ($m = 1, E_1 \leq E \leq E_0, E_0 = \infty$) (see Figure 1 in refs 12 and 13), $1/2^2$ for the

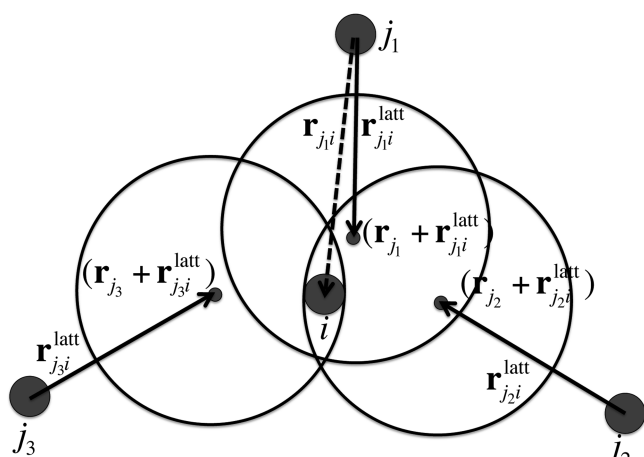


Figure 1. A simple two-dimensional example to depict the cage model. i is the central molecule, and j_1, j_2 , and j_3 are its nearest neighbors. $\mathbf{r}_{ji}^{\text{latt}}$ is an ideal lattice vector, \mathbf{r}_{ji} is an intermolecular vector, and molecule i is restricted to the intersection of the circles centered at $\mathbf{r}_j + \mathbf{r}_{ji}^{\text{latt}}$, for $j = \{j_1, j_2, j_3\}$.

second subdivision ($m = 2, E_2 \leq E \leq E_1$), and so on down to $1/2^n$ for the two lowest-energy subdivisions ($m = n, E_n \leq E \leq E_{n-1}$ and $m = n+1, -\infty \leq E \leq E_n$).

For the n^{th} division of the density of states (to produce energy boundary E_n), MC sampling is performed with a discrete weighting function $w(E) = 4^m$ for the previously calculated subdivisions $m < n$ (subdivision 1 being the highest energy). The first division of the energy (to produce the energy boundary E_1), $n = 1$, does not employ any weighting function (random sampling). For larger n , the weighting function is essential to speed up the simulations; it ensures that about 2/3 or more of the configurations of the system fall into the current lowest-energy subdivision.¹² At the end of a predetermined number of MC moves, the energy boundary E_n is set equal to the median configurational energy found in the lowest-energy subdivision $-\infty \leq E \leq E_{n-1}$, and all sampled energies are discarded. The simulation is repeated to find as many energy subdivisions as required. Details on the stopping criterion can be found in our previous work.^{12,13} The excess partition function (Q_{ex}) is obtained from the normalized integrated density of states as $Q_{\text{ex}} = \sum_{m=1}^{m=n+1} 2^{-m} \exp(-\beta \langle E \rangle_m) / \sum_{m=1}^{m=n+1} 2^{-m}$ (Figure 2a), where $\langle E \rangle_m = (E_m + E_{m-1})/2$. For the first energy

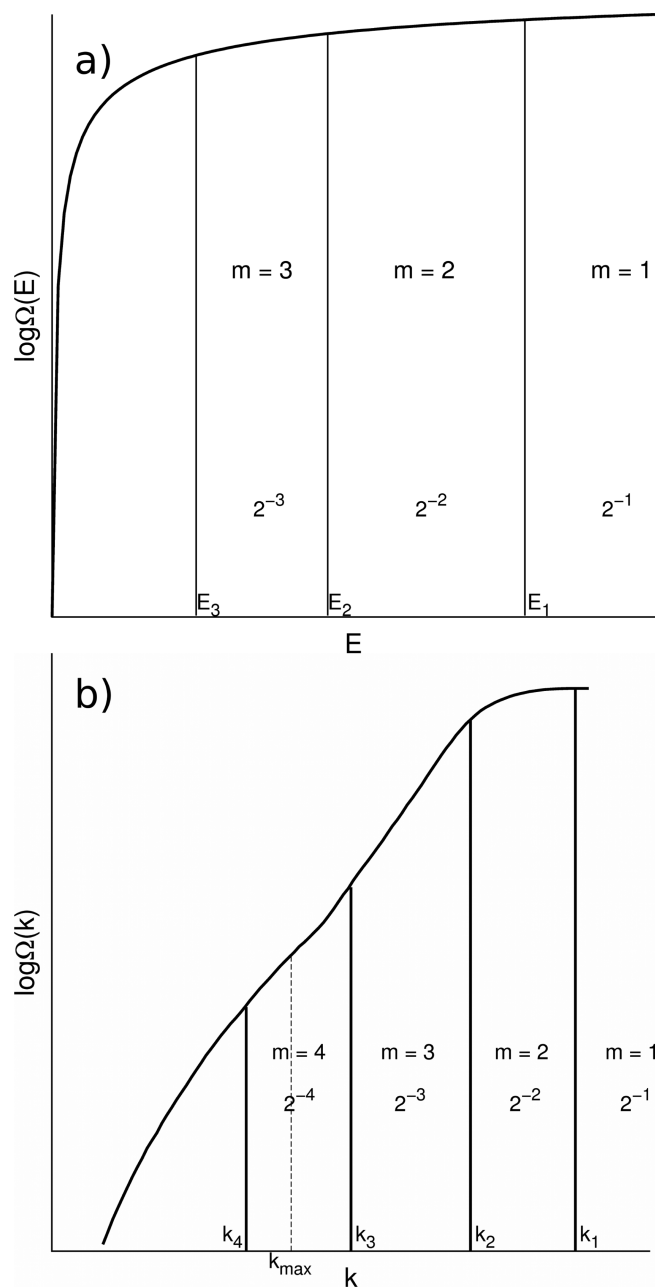


Figure 2. Schematic (not to scale) explaining the partitioning of the density of states for (a) an interacting system (partitioning E) and (b) for a noninteracting system (partitioning k) with $n = 4$. m labels the DOS partitions.

subdivision ($m = 1$), $\langle E \rangle_m$ is set equal to E_1 , and for the last energy subdivision, $\langle E \rangle_m$ is set equal to E_n . Also, in the last energy subdivision, 2^{-m} is replaced by 2^{-n} , as the normalized integrated density of states of the two lowest-energy subdivisions are the same and equal to 2^{-n} .

Continuous Weighting Functions. The drawback of the above weighting function is that the discontinuous weights $w(E)$ may reduce the likelihood of the system moving between energy subdivisions. To circumvent this, we propose a new continuous weighting function $w(E) = \exp(-3 \log_2(E - E_{n-1}) / (E_{n-2} - E_{n-1}))$ for the n^{th} division of the density of states when $n \geq 3$ and $E \geq E_{n-1}$; $w(E) = 1$ for the first two divisions $n = 1, 2$, and whenever $E < E_{n-1}$. This weighting function is designed such that if the density of states $\Omega(E)$ is roughly exponential near E_n ,

about 2/3 of the configurations of the system fall into the current lowest-energy subdivision. The probability of accepting a move from an old state with configurational energy E_{old} to a new state with configurational energy E_{new} , using the Metropolis acceptance criterion, is

$$P(\text{old} \rightarrow \text{new}) = \min[1, w(E_{\text{new}})/w(E_{\text{old}})] \quad (1)$$

It is important to note that the continuous weighting function does not add any bias to the density of states calculations, because it is always equal to one in the sampled region.

CALCULATING THE FREE ENERGY OF A SOLID

The density of states of a solid is small compared to that of a liquid, and the DOS partitioning method cannot locate the correct structure of a solid: it finds supercooled liquid structures instead. Nested Sampling with many walkers may be able to find solid structures for small numbers of particles,¹⁴ but this could require a great increase in computational expense. Thus, a guided simulation with a good order parameter is useful to partition the configuration space of solids.

The free energy of a solid is expressed as $F = F_{\text{id}} + F_{\text{ex}}$ where F_{id} and F_{ex} are the ideal gas and excess free energies, respectively. The excess free energy is separated into two contributions: F_{ex}^1 and F_{ex}^2 . F_{ex}^1 is the excess free energy of a noninteracting solid with respect to the ideal gas, and F_{ex}^2 is the excess free energy of an interacting solid with respect to the noninteracting solid. F_{ex}^2 can be obtained by utilizing the DOS partitioning approach^{12,13} with the reference system being the noninteracting solid. F_{ex}^1 for many solid models including the cell¹⁶ and Einstein crystal¹⁷ models can be calculated exactly. However, if a solid model that does not have an exact expression for F_{ex}^1 is used, one has to calculate F_{ex}^1 and our DOS partitioning approach is suitable for this task.

The Cage Model for a Solid. In this work, we propose a new solid model, which we refer to as a "cage model". It can be applied to a general solid, for which each molecule i is surrounded by neighbors j in the perfect crystal. The number of neighbors in the cage model is determined based on the type of perfect crystal (e.g., 12 for FCC lattice). We denote the ideal lattice vectors from j to i as $\mathbf{r}_{ji}^{\text{latt}}$ and the actual intermolecular vectors during the simulation as \mathbf{r}_{ji} . The cage model restricts all "neighbor" vectors \mathbf{r}_{ji} such that $|\mathbf{r}_{ji} - \mathbf{r}_{ji}^{\text{latt}}| \leq k_{\text{max}} |\mathbf{r}_{ji}^{\text{latt}}|$, where k_{max} is a constant that is determined empirically. Figure 1 shows a simple example of a molecule i and three of its "neighbors" j_{1-3} . In the cage model, each particle i is constrained (caged) in a region which is formed by the intersection of several spheres of radius $k_{\text{max}} |\mathbf{r}_{ji}^{\text{latt}}|$. Note that if k_{max} is large, the molecules i and j may not be nearest neighbors during the simulation. When $k_{\text{max}} = \infty$, the system is not constrained at all by the cage model. Nevertheless, the same ij pairs are treated as "nearest neighbors" within the cage model; the neighbor list does not need to be updated. As k_{max} is reduced, the structure of the solid is formed.

F_{ex}^1 for the cage model can be calculated by partitioning its geometrical configuration space with respect to the ideal gas (molecule number 1 is fixed, for convenience). We partition the configuration space as a function of k , which is $\max_{ij} (|\mathbf{r}_{ji} - \mathbf{r}_{ji}^{\text{latt}}| / |\mathbf{r}_{ji}^{\text{latt}}|)$ for all "nearest neighbor" pairs ij . In this case, k takes the place of the configurational energy in the DOS partitioning approach. A schematic of the partitioning process of both E and k is shown in Figure 2. The partitioning process is terminated when $k \leq k_{\text{max}}$. If the last boundary k_n equals k_{max} then Q_{ex}^1 (the

fraction of the configurational space of the ideal gas that obeys the cage model) equals $N!/2^n$, where n is the number of partitions and the factor $N!$ is due to indistinguishability. However, it is very unlikely that $k_n = k_{\text{max}}$ by chance. In practice, $k_n < k_{\text{max}}$ and then $Q_{\text{ex}}^1 = N! \times f/2^{n-1}$, where $f = N_{\text{config}}(k < k_{\text{max}}) / N_{\text{config}}(k < k_{n-1})$. At the end of the partitioning process, F_{ex}^1 is calculated as $F_{\text{ex}}^1 = -k_B T \log_e Q_{\text{ex}}^1$.

The Cage versus the Cell Model. A good model for a solid is one that can describe the real solid under a broad range of conditions, especially at low density and high temperature, and that has a small configuration space. In the cage model, the constant k_{max} must be specified. k_{max} should be large enough so that the model can capture all of the equilibrium distribution of the real solid configurations, but at the same time it should be kept as small as possible to maintain a small configuration space. In the cell model, the volume V of the simulation box is divided into N Wigner-Seitz cells¹⁶ representative of the solid phase under consideration. The cell model restricts all particles i to stay within their cells, such that $|\mathbf{r}_i - \mathbf{r}_i^{\text{latt}}| \leq |\mathbf{r}_i - \mathbf{r}_j^{\text{latt}}| \forall j$. The fraction of the ideal gas that obeys the cell model is known exactly. To compare the cage against the cell model, we consider a FCC 12–6 Lennard-Jones solid. The cage model uses 12 "neighbors" for each molecule. We perform a set of NVT MC simulations of the solid using 500 particles at two points near the phase transition line: one is near the triple point (low density $\rho^* = 0.98$ and low temperature $T^* = 0.70$) and one is above the critical point (low density $\rho^* = 1.12$ and high temperature $T^* = 2.0$). At each point in phase space, we calculate the fraction of configurations encountered in the simulation that obey the cell and cage models. Figure 3a shows that for $k_{\text{max}} \geq 0.70$ more than 99.93% of the configurations obey the cage model under both conditions, while at high temperature ($T^* = 2.0$) the cell model only captures about 97% of the configurations of the solid.

In order to compare the configuration space of the noninteracting cell and cage models, we calculate Q_{ex}^1 (by partitioning k) of the cage model (Q_{cage}) for each value of k_{max} using 500 noninteracting particles and compare it with the Q_{ex}^1 of the cell model (Q_{cell}). Figure 3b shows that the total ideal gas configuration space of the cage model is smaller than that of the cell model for $k_{\text{max}} \leq 0.92$. Thus, we can conclude that the cage model is better than the cell model for FCC solids if $0.7 \leq k_{\text{max}} \leq 0.92$. It not only better represents the equilibrium distribution of solid configurations (Figure 3a) but also has a smaller configuration space (Figure 3b).

Calculating Q_{ex}^1 of the Cage Model. Since both the cell and cage models attempt to represent the equilibrium distributions of solid configurations, their configuration spaces overlap (Figure 4). Partitioning the configuration space of the cage model with respect to the ideal gas requires a substantial number of MC steps for each division of k , because the probability of changing k is small in each step (of order $1/N$). Therefore, we propose a different route to calculate Q_{ex}^1 efficiently for the cage model (Q_{CD} in Figure 4) using the exact value of Q_{BC} (Q_{ex}^1 of the cell model). For this, we need to calculate the fraction of the configuration space of the cell model that obeys the cage model ($Q_{\text{C}}/Q_{\text{BC}}$) and the fraction of the configuration space of the cage model that obeys the cell model ($Q_{\text{C}}/Q_{\text{CD}}$). Hence, the configuration space of the ideal gas that obeys the cage model (Q_{CD}) is calculated as $Q_{\text{CD}} = Q_{\text{BC}}(Q_{\text{C}}/Q_{\text{BC}})/(Q_{\text{C}}/Q_{\text{CD}})$. To calculate $(Q_{\text{C}}/Q_{\text{BC}})$, we partition k of the cage model and reject any configuration that does not obey the cell model. To calculate $(Q_{\text{C}}/Q_{\text{CD}})$, we partition $r_{\text{max}}^{\text{cell}}$

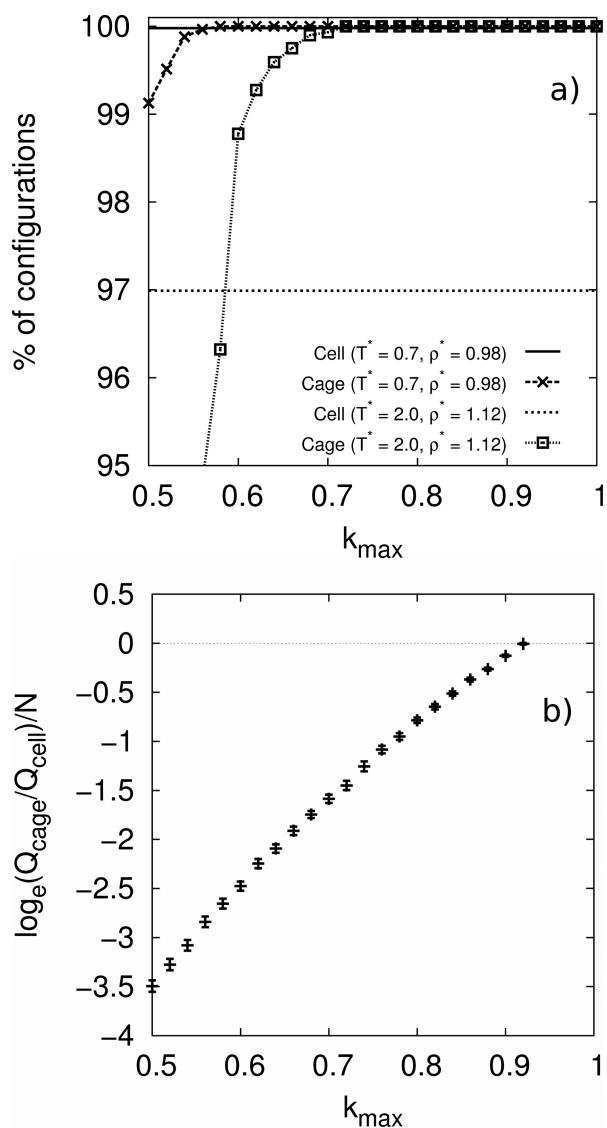


Figure 3. a) Percentage of solid configurations from NVT MC simulations of Lennard-Jones solid that obey the cell and cage models versus the size of the cage (k_{\max}). b) Total ideal gas configuration space difference between the cage and the cell models versus the size of the cage (k_{\max}).

of the cell model, which is $\max_{ij}(|r_i - r_i^{\text{latt}}| - |r_i - r_j^{\text{latt}}|)$ for all N particles i and their 12 nearest neighbors j . We reject any configuration that does not obey the cage model and stop the partitioning process when $r_{\max}^{\text{cell}} < 0$.

■ CASE STUDY FOR DRY ICE

To demonstrate our new technique, we calculate the partition function, free energy, and solid–fluid equilibrium properties of CO_2 . The two most popular force fields for CO_2 (EPM³² and TraPPE³³) are employed. Both of these force fields have been extensively used in simulations of fluids. However, they have not been fully tested for simulations involving the solid phase. The excess free energy of the fluid phase (F_{ex}^f) is calculated using our previous algorithm.^{12,13} Simulations for the solid phase are performed in a cubic box using 500 molecules with periodic boundary conditions. The starting configuration for all simulations is the FCC structure of dry ice. To obtain a value for the k_{\max} constant, we perform a similar analysis to the

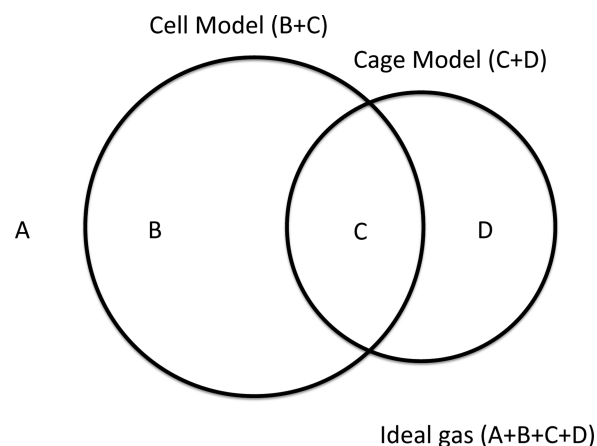


Figure 4. Sketch (not to scale) of the configuration spaces of the ideal gas ($A + B + C + D$), noninteracting cell model ($B + C$), and noninteracting cage model ($C + D$). Q_{BC} is Q_{ex}^1 of the cell model, Q_{CD} is Q_{ex}^1 of the cage model, and Q_C is Q_{ex}^1 of the overlapping region between Q_{BC} and Q_{CD} .

Lennard-Jones solid (described in the previous section) (Figure 3a). Nearest neighbor distances are calculated using the carbon atom positions. We find that $k_{\max} = 0.75$ is sufficient to capture over 99.99% of the solid configurations under all studied conditions. A spherical cutoff of half of the length of the simulation box is used to truncate the Lennard-Jones interactions. Thus, a long-range correction for the r^{-6} term (tail correction) is used: $E_{\text{tail}} = -64\pi\rho\epsilon\sigma^6/3V$, where ρ and V are the density and volume of the simulation box, respectively, ϵ is the potential energy well depth, and σ is the core diameter. The r^{-12} term decays rapidly with distance, so a correction for this term is unnecessary. The quadrupole–quadrupole interactions are sufficiently short-ranged that a long-range correction for the electrostatic energy is not needed.

F_{ex}^1 of the cage model is a universal constant; it only depends on the lattice type and the number of molecules. Table 1 gives Q_{ex}^1 ($F_{\text{ex}}^1 = -k_B T \log_e Q_{\text{ex}}^1$) for the cage model along with Q_{BC} , Q_C/Q_{BC} , and Q_C/Q_{CD} for a different number of particles in a FCC lattice (see Figure 5).

For CO_2 , we restrict the molecular rotation to $\theta \leq \theta_{\max}$ from the ideal-lattice angles and add $F_{\text{rot}} = -k_B T \log_e(0.5 - 0.5 \cos \theta_{\max})$ to the excess free energy. F_{rot} is the rotational free energy of the noninteracting system due to orientation restriction. In the case of CO_2 , we also add $F_{\text{sym}} = -k_B T N \log_e 2$ to the excess free energy to account for indistinguishability due to the symmetry of the CO_2 molecule. To calculate θ_{\max} we perform a set of NVT MC simulations in the solid phase (using 500 molecules) at various temperatures in the range 150–400 K and accumulate histograms of $\cos \theta = \mathbf{r}_{\text{mol}}^{\text{id}} \cdot \mathbf{r}_{\text{mol}}$. We find that on average less than 0.0001% of the configurations have $\theta \geq 40^\circ$. Thus, we set $\theta_{\max} = 40^\circ$.

F_{ex}^2 is calculated by partitioning the energy of the interacting cage model with the restriction that $\theta < 40^\circ$. Figure 5 shows the free energies of the solid ($F^{\text{id}} + F_{\text{ex}}^1 + F_{\text{ex}}^2 + F_{\text{rot}} + F_{\text{sym}}$) and fluid ($F^{\text{id}} + F_{\text{ex}}^f$) phases per particle versus volume per particle for 500 CO_2 (TraPPE model) molecules at 260 K. The coexisting volumes are determined by constructing a double tangent. The coexisting pressure is the slope of this tangent line. The latent heat of fusion (or sublimation) equals $(\langle E \rangle_f - \langle E \rangle_s) + p(V_f - V_s)$, where $\langle E \rangle$ is the ensemble average of the energy (see ref 12).

The sublimation and fusion pressure lines calculated for CO_2 using the EPM and TraPPE models are compared to

Table 1. Universal Constants for the Cage Model ($k_{\max} = 0.75$) for Different Number of Particles in a FCC lattice^a

N	$\log_e Q_{ex}^1$	$(\log_e Q_{ex}^1)/N$	$\log_e Q_{BC}$	$\log_e [Q_C/Q_{BC}]$	$\log_e [Q_C/Q_{CD}]$
32	-48.1 (0.4)	-1.50 (0.01)	-32.00	-19.7 (0.2)	-3.6 (0.1)
108	-170.4 (1.2)	-1.58 (0.01)	-108.0	-69.6 (0.8)	-7.2 (0.4)
256	-409.4 (2.9)	-1.60 (0.01)	-256.0	-166.0 (1.5)	-12.7 (1.8)
500	-800.9 (4.4)	-1.60 (0.01)	-500.0	-322.0 (3.4)	-21.1 (0.9)
864	-1383.0 (7.3)	-1.60 (0.01)	-864.0	-552.8 (5.9)	-33.8 (1.2)

^aNumbers in parentheses are standard deviations.

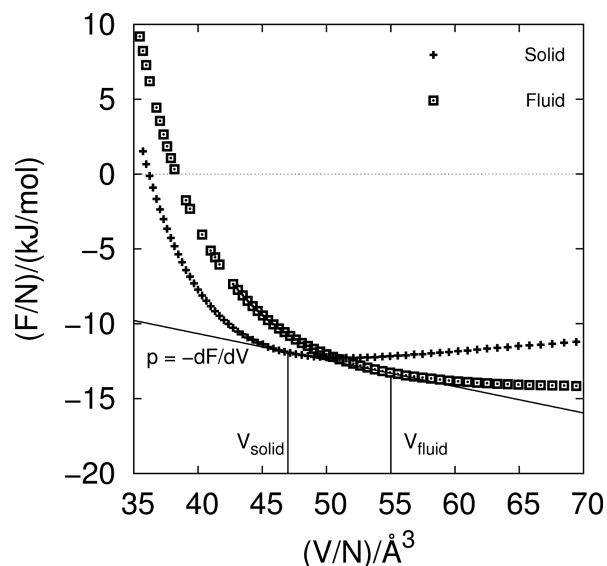


Figure 5. Helmholtz free energy per particle versus volume per particle of CO₂ (TraPPE) at 260 K. The error bars are too small to show on the plot.

experimental data^{34,35} in Figures 6 and 7. Over the entire temperature range, the TraPPE model shows a good agreement with experiments, while the EPM model only agrees at low temperature and gradually overestimates the sublimation and fusion pressure as the temperature increases. It is encouraging to see that the relatively simple, nonpolarizable TraPPE force field for CO₂ that was developed by fitting to high-temperature

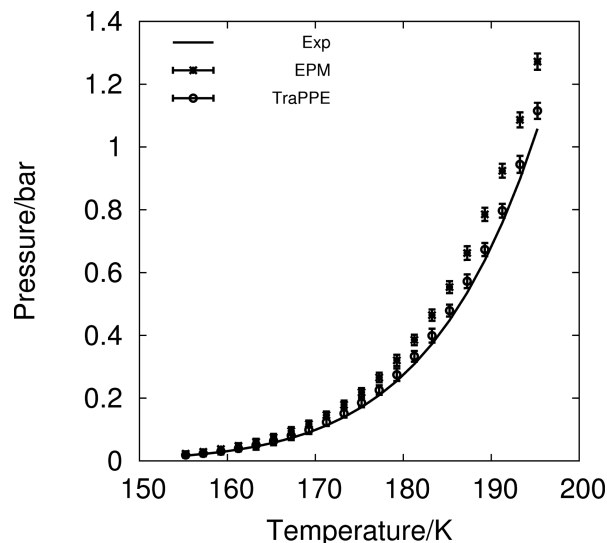


Figure 6. Solid–vapor equilibrium of CO₂: experiment (solid line),³⁴ EPM force field (star), and TraPPE force field (circle).

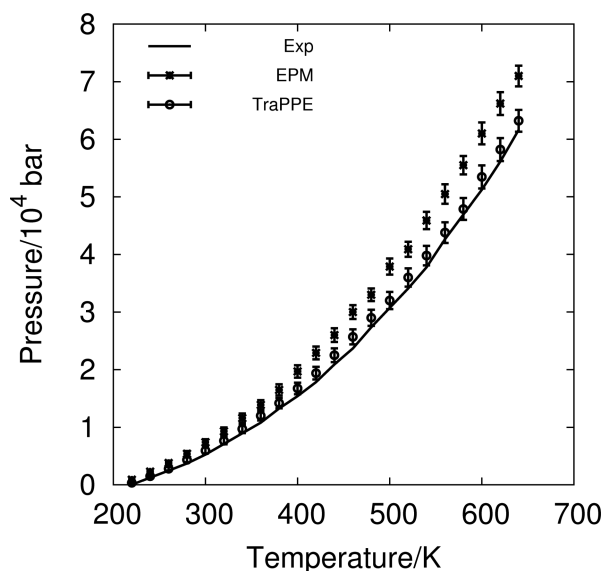


Figure 7. Solid–liquid equilibrium of CO₂: experiment (solid line),³⁵ EPM force field (star), and TraPPE force field (circle).

vapor–liquid equilibria can also be applied to study the solid phase under a wide range of conditions.

Our calculated triple point is $T_T = 213 \pm 2$ K and $p_T = 4.1 \pm 0.3$ bar for the TraPPE model, which agrees with simulated data from the literature.³⁶ The triple point predicted by the EPM force field is $T_T = 205 \pm 3$ K and $p_T = 2.5 \pm 0.3$ bar. These values are slightly below their experimental counterparts (216.6 K and 5.18 bar, respectively³⁷) due to the overestimation of the sublimation pressure.

The available data for the enthalpy of sublimation of CO₂^{34,38,39} are compared with our simulations using the TraPPE and EPM force fields in Figure 8. Both force fields slightly overestimate the heat of sublimation and EPM provides a better prediction. For the enthalpy of fusion at the triple point, our simulations yield a value of 7.9 ± 0.4 kJ/mol using the TraPPE force field and 7.0 ± 0.4 kJ/mol using the EPM force field, while the reported equation of state and experimental values are 8.05, 8.34, 7.95, and 8.87 kJ/mol.^{38,39} Figure 9 compares the change in molar volume on melting with the predictions obtained from the equations of state for the solid³⁸ and liquid⁴⁰ phases and the experimental data of Bridgman.⁴¹ There is good agreement with the experimental data and equation of state at all pressures, although the simulated values are slightly lower. On the other hand, the equations of state slightly overestimate the experimental volume change. The TraPPE force field continues to perform better than EPM. The predicted change in volume upon melting by this force field is very close to experiment.

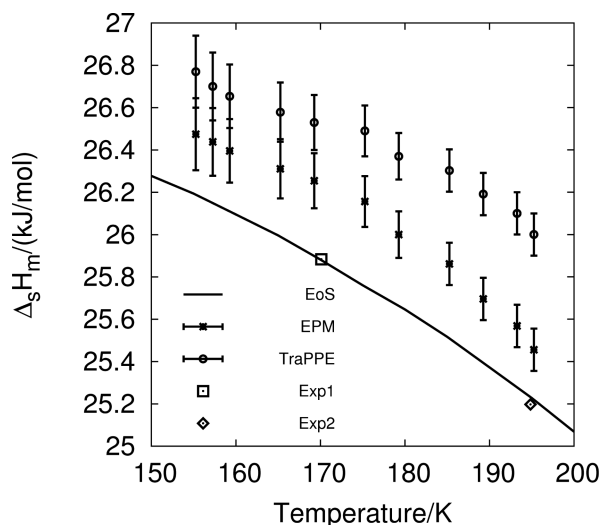


Figure 8. Latent heat of sublimation of CO₂: equation of state (solid line),³⁸ experiment 1 (square),³⁴ experiment 2 (diamond),³⁹ EPM force field (star), and TraPPE force field (circle).

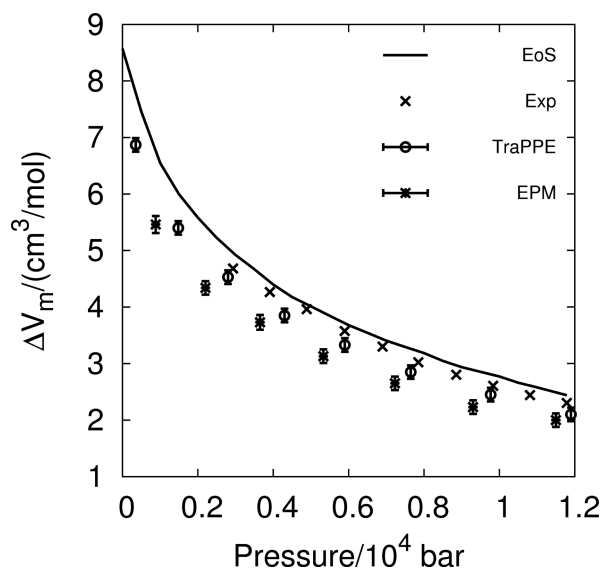


Figure 9. Change in volume upon melting of CO₂: equation of state (solid line),^{38,40} experiment (cross),⁴¹ EPM force field (star), and TraPPE force field (circle).

CONCLUSION

In summary, we have developed a new technique, which combines a cage model and an DOS partitioning approach, to compute the excess free energy of an arbitrary solid. We apply our method to calculate the excess free energy of CO₂ cubic phase I (dry ice) and predict its solid–vapor and solid–liquid phase transition using the EPM and TraPPE force fields. Our cage model for the solid has a better performance than the cell model, because it better represents the equilibrium distributions of solid configurations, while having a smaller configuration space than that of the cell model. The excess free energy of the noninteracting cage model is a universal lattice constant, which only depends on the lattice type and the number of molecules. That means this quantity only needs to be calculated once and then can be used for any crystalline system.

In general, the agreement between simulated data, experiment and equations of state is satisfactory. Simulations slightly

overestimate the sublimation pressure, fusion pressure, and heat of sublimation, while they slightly underestimate both T_T and p_T (triple point), heat of fusion, and the volume changes upon melting. Overall, the TraPPE force field performs better than EPM, in terms of predicting the free energy of the solid and the solid–fluid phase transition properties. Future work will involve the study of solid–solid phase transitions and predicting high-pressure structures of CO₂.

Since the partition function (and hence free energy) is obtained from the density of states, which is independent of the temperature, equilibrium thermodynamic properties at any condition can be obtained by varying the density. This makes our method efficient in comparison to other free energy techniques. The DOS partitioning method is not limited to the study of phase equilibria; it can also be applied to calculate solvation free energies, nucleation dynamics, and properties of systems with discrete energy levels, including spin glasses and lattice models of proteins and polymers.

AUTHOR INFORMATION

Corresponding Author

*E-mail: hainam.do@nottingham.ac.uk (H.D.), richard.wheatley@nottingham.ac.uk (R.J.W.).

Notes

The authors declare no competing financial interest.

ACKNOWLEDGMENTS

We thank the University of Nottingham High Performance Computing facility for providing computer resources and the Engineering and Physical Sciences Research Council (EPSRC) for funding (Grant No. EP/E06082X). We are grateful to Prof. Jonathan Hirst for useful comments on the manuscript.

REFERENCES

- (1) Hansen, J.; Verlet, L. *Phys. Rev.* **1969**, *184*, 151–161.
- (2) White, R. P.; Meirovitch, H. *Proc. Natl. Acad. Sci. U.S.A.* **2004**, *101*, 9235–9240.
- (3) Tyka, M. D.; Sessions, R. B. *J. Phys. Chem. B* **2007**, *111*, 9571–9580.
- (4) Torrie, G. M.; Valleau, J. P. *J. Chem. Phys.* **1977**, *66*, 1402–1408.
- (5) Ferrenberg, A. M.; Swendsen, R. H. *Phys. Rev. Lett.* **1989**, *63*, 1195–1198.
- (6) Berg, B.; Neuhaus, T. *Phys. Lett. B* **1991**, *267*, 249–253.
- (7) Wang, J. S.; Tay, T. K.; Swendsen, R. H. *Phys. Rev. Lett.* **1999**, *82*, 476–479.
- (8) Wang, F. G.; Landau, D. P. *Phys. Rev. Lett.* **2001**, *86*, 2050–2053.
- (9) Yan, Q.; Faller, R.; de Pablo, J. J. *J. Chem. Phys.* **2001**, *116*, 8745–8749.
- (10) Shell, M. S.; Debenedetti, P. G.; Panagiotopoulos, A. Z. *J. Chem. Phys.* **2003**, *119*, 9406–9411.
- (11) Ganzenmuller, G.; Camp, P. J. *J. Chem. Phys.* **2007**, *127*, 154504–154513.
- (12) Do, H.; Hirst, J. D.; Wheatley, R. J. *J. Chem. Phys.* **2011**, *135*, 174105–174111.
- (13) Do, H.; Hirst, J. D.; Wheatley, R. J. *J. Phys. Chem. B* **2012**, *116*, 4535–4542.
- (14) Partay, L. B.; Bartok, A. P.; Csanyi, G. *J. Phys. Chem. B* **2010**, *114*, 10502–10512.
- (15) Burkoff, N. S.; Varnai, C.; Wells, S. A.; Wild, D. L. *Biophys. J.* **2012**, *102*, 878–886.
- (16) Hoover, W. G.; Ree, F. H. *J. Chem. Phys.* **1968**, *49*, 3609–3617.
- (17) Frenkel, D.; Ladd, A. J. C. *J. Chem. Phys.* **1984**, *81*, 3188–3193.
- (18) Oakley, M. T.; Wheatley, R. J. *J. Chem. Phys.* **2009**, *130*, 34110–34119.

- (19) Oakley, M. T.; Do, H.; Wheatley, R. J. *Fluid Phase Equilib.* **2009**, *290*, 48–54.
- (20) Oakley, M. T.; Do, H.; Hirst, J. D.; Wheatley, R. J. *J. Chem. Phys.* **2011**, *134*, 114518–114525.
- (21) Do, H.; Wheatley, R. J.; Hirst, J. D. *J. Phys. Chem. B* **2010**, *114*, 3879–3886.
- (22) Do, H.; Wheatley, R. J.; Hirst, J. D. *Phys. Chem. Chem. Phys.* **2011**, *13*, 15708–15713.
- (23) Sun, J.; Klug, D. D.; Martonak, R.; Montoya, J. A.; Lee, M.; Scandolo, S.; Tosatti, E. *Proc. Natl. Acad. Sci. U.S.A.* **2008**, *106*, 6077–6081.
- (24) Iota, V.; Yoo, C.; Klepeis, J.; Jenei, Z.; Evans, W.; Cynn, H. *Nat. Mater.* **2007**, *6*, 34–38.
- (25) Santoro, M.; Gorelli, F. A.; Bini, R.; Ruocco, G.; Scandolo, S.; Crichton, W. A. *Nature* **2006**, *441*, 857–860.
- (26) Gorelli, F. A.; Giordano, V. M.; Salvi, P. R.; Bini, R. *Phys. Rev. Lett.* **2004**, *93*, 205503–205507.
- (27) Tschauner, O.; Mao, H.-K.; Hemley, R. J. *Phys. Rev. Lett.* **2001**, *87*, 75701–75704.
- (28) Iota, V.; Yoo, C. S.; Cynn, H. *Science* **1999**, *283*, 1510–1513.
- (29) Bonev, S. A.; Gygi, F.; Ogitsu, T.; Galli, G. *Phys. Rev. Lett.* **2003**, *91*, 65501–65504.
- (30) Holm, B.; Ahuja, R.; Belonoshko, A.; Johansson, B. *Phys. Rev. Lett.* **2000**, *85*, 1258–1211.
- (31) Serra, S.; Cavazzoni, C.; Chiarotti, G. L.; Scandolo, S.; Tosatti, E. *Science* **1999**, *284*, 788–790.
- (32) Harris, J. G.; Yung, K. H. *J. Phys. Chem.* **1995**, *99*, 12021–12024.
- (33) Potoff, J. J.; Siepmann, J. I. *AIChE J.* **2001**, *47*, 1676–1682.
- (34) Giaque, W. F.; Egan, C. J. *J. Chem. Phys.* **1937**, *5*, 45–54.
- (35) Giordano, V. M.; Datchi, F.; Dewaele, A. *J. Chem. Phys.* **2006**, *125*, 54504–54511.
- (36) Chen, B.; Siepmann, J. I.; Klein, M. L. *J. Phys. Chem. B* **2001**, *105*, 9840–9848.
- (37) Lemmon, E. W.; McLinden, M. O.; Friend, D. G. Thermophysical Properties of Fluid Systems. In *NIST Chemistry WebBook*; NIST Standard Reference Database Number 69; Mallard, W. G., Linstrom, P. J., Eds.; National Institute of Standards and Technology: Gaithersburg, MD, 2000. <http://webbook.nist.gov>.
- (38) Trusler, J. P. M. *J. Phys. Chem. Ref. Data* **2011**, *40*, 43105–43123.
- (39) Maass, O.; Barnes, W. H. *Proc. R. Soc. London, Ser. A* **1926**, *111*, 224–244.
- (40) Span, R.; Wagner, W. J. *Phys. Chem. Ref. Data* **1996**, *25*, 1509–1596.
- (41) Bridgman, P. W. *Phys. Rev.* **1914**, *3*, 153–203.